J. Appl. Comput. Mech., 5(5) (2019) 861-874
DOI: 10.22055/JACM.2019.28043.1452

ISSN: 2383-4536
jacm.scu.ac.ir

M&MoCS

Shahid Chamran University of Ahvaz

Journal of Applied and Computational Mechanics

Research Paper

Numerical Analysis of the Effect of External Circumferential Elliptical Cracks in Transition Thickness Zone of Pressurized Pipes Using XFEM

Houda Salmi[1], Khalid El Had[2], Hanan El Bhilat[1], Abdelilah Hachim[2]

[1] National Higher School of Mechanics, ENSEM, Laboratory of Control and Mechanical Characterization of Materials and Structures, Casablanca, Morocco

[2] Institute of Maritims Studies, Laboratory of Materials and Structures, Casablanca, Morocco

Received December 29 2018; Revised May 05 2019; Accepted for publication May 06 2019.
Corresponding author: Salmi Houda, h.salmi@ensem.ac.ma

Abstract. The present work investigates the effect of the elliptical three-dimensional (3D) cracks on a pipe with thickness transition, considering internal pressure. Level sets were defined using the extended finite element method (XFEM), the stress intensity factors (SIFs) of 3D cracks were investigated and compared between straight pipes and pipes with thickness transition. The results show that the XFEM is an effective tool for modeling crack in pipes. A pressurized pipe with thickness transition is more sensitive to the feature compared to the straight pipe. Parameters of the transition zone have an influence on stress intensity factors. Quantification of the SIFs associated with cracks in the transition zone of pipes with thicknesses is performed.

Keywords: Pressurized equipment, Pipe with thickness transition, Three-dimensional crack, XFEM, SIF, Level set.

1. Introduction

In industrial sectors, pipes are often presented as an economical and safe means of transporting oil and gas. However, those structures are exposed to rupture accidents [1, 2]. In the field of pressure equipment, cylindrical or spherical structures are often found, those shells can be affected by axisymmetric or semi-elliptical internal or external cracks, it is then very important to evaluate the effect of these cracks on pressure equipment [3]. Xiao et al. [4] investigated the fatigue crack growth of offshore pipelines affected by 3D cracks, Shidar et al. [5] considered the plastic behavior to study girth welded pipelines with 3D cracks exposed to biaxial loadings. In the elastic range, the problem of the cracks is generally studied using the SIF [6, 7]. Philippe [8] used the finite element method (FEM) to investigate the SIF of a semi-elliptical defect in a cylindrical shell. Sabokrooh et al. [9] studied the effect of residual stresses of the girth welding on a pipe of gas transmission. Vakili Tahami et al. [10] applied the harmony search algorithm to give the optimum designs of functionally graded-carbon -reinforced pipes exposed to a moving load.

The French Alternative Energies and Atomic Energy Commission (CEA) [11] developed the software for calculating finite element structures Castem [12]. The CEA [11, 13] launched studies with FEM to evaluate uniform thickness pipes containing internal and external circumferential cracks.

The field of pressure equipment deals also with thickness transition pipes, these pipes correspond to a connection between two cylinders of the same internal radius but with different thicknesses. Those structures are subjected to circumferential cracks at the base of the thickness transition. Those defects are modeled as cracks located in a pipe of uniform thickness t [14].

Using the FEM, Delliou [15] studied pipe with thickness transition containing axisymmetric crack subjected to tensile stress and/or thermal shock, while Saffih [14] extended the study to semi-elliptic crack considering bending moment and

Published online: May 24 2019

tensile stress. The results obtained in refs. [14, 15] showed that for elastic material, the thickness transition zone is the weakest position of the whole pipe.

Since the traditional FEM approach is more cumbersome in the modeling of crack because of mesh refinement, the accuracy of the results in the FEM depends on the mesh, a fine mesh near the tip of the crack allows a precise result. However, a fine mesh implies a large number of meshes and nodes, so it requires a long time of calculation [13], hence the introduction of the XFEM to facilitate the solving of cracks problems that are not efficiently resolved by mesh refinement.

The XFEM is used to analyze in 3D, the external circumferential elliptical cracks in the thickness transition zone, in this method, the finite element basis is enriched by specific functions that describe the surface and the tip of the crack, those functions allow additional precision in the modeling of the stationary defect and the crack growth [16, 17]. For stationary cracks, the XFEM gives an accurate result, thanks to enrichment functions even with coarse meshes near the crack tip [16]. The XFEM was initiated by Belytschko and Black [18]. Stolarska et al. [19] proposed the coupling between the level set met hod (LSM) and XFEM to investigate the problem of cracks. In the field of pressurized equipment, Sharma [20] used the XFEM to evaluate the SIFs of a semi-elliptical crack in pipe bend.

Using the XFEM to compare the effect of the 3D crack between straight pipes and those with thickness transition besides evaluating the effect of transition zone on SIF were however not treated in [14], also, taking account of internal pressure was required to complete the work done by Saffih and Hariri [14]. The purpose of this work is to demonstrate the application of XFEM to evaluate the effect of 3D external elliptical crack on a pipe with thickness transition and investigate the impact of this transition zone on SIF of the cracked pipe. A study with a numerical simulation software Castem [12] was performed considering internal pressure.

In section 2, a description of XFEM in a matrix form is introduced. The definition of enrichment zone and the level set is provided. The theoretical method to calculate the SIF using XFEM is given. In section 3, the geometry of the pressurized equipment is defined. In section 4, XFEM model verification is validated. The influence of the transition zone on the SIF is investigated, at the same time, optimization of the transition zone dimensions based on the minimum SIF of the cracked pipe is discussed. Finally, a comparative study of SIF is done between straight pipes and pipes with thickness transition.

2. XFEM Methodology

2.1. XFEM formulation

In XFEM, the standard finite element approximation is locally enriched to discontinuities modeling. At a particular node x_i, the displacement approximation U is given by Eq. (1) [16]:

$$U(x)=\sum_{i\in N}N_i(x)u_i+\sum_{i\in N_d}N_i(x)(H(x)-H(x_i))a_i+\sum_{i\in N_p}[N_i(x)(\sum_{\alpha=1}^{4}(\beta_\alpha(x)-\beta_\alpha(x_i))b_i^\alpha)] \tag{1}$$

where, N_i is the standard finite element (FE) function of node i, u_i is the unknown displacement of the standard FE part at node i, N is the set of all nodes in the domain and $N_d \subset N$ denotes the nodal subset of the enrichment Heaviside function $H(x)$, which is defined for those elements that are entirely cut by the crack surface and we have:

$$H(x)=\begin{cases}1 & \text{if } \varphi(x)>0\\ -1 & \text{otherwise}\end{cases} \tag{2}$$

where $\varphi(x)$ is the normal level set function and a_i denotes the unknown of the enrichment $H(x)$ at node i, these nodes are surrounded by a square in Fig. 1; and $N_p \subset N$ is the nodal subset of the enrichment β_α which is defined for those elements that are partly cut by the crack front, the tip of the crack is described by four enrichment functions [16]:

$$\{\beta_\alpha(r,\theta)\}=\{\beta_1,\beta_2,\beta_3,\beta_4\}=\left\{\sqrt{r}\sin\left(\frac{\theta}{2}\right),\sqrt{r}\cos\left(\frac{\theta}{2}\right),\sqrt{r}\sin\left(\frac{\theta}{2}\right)\sin(\theta),\sqrt{r}\cos\left(\frac{\theta}{2}\right)\sin(\theta)\right\} \tag{3}$$

in which $r=\sqrt{(\varphi^2+\psi^2)}$ and $\theta=\tan^{-1}(\varphi/\psi)$ with φ and ψ are respectively the normal and tangential level sets, b_i is the unknown of the enrichment β_α at node i, these nodes are surrounded by a circle in Fig. 1.

2.2. Castem definition

Cast3M (Castem) [12] is a numerical simulation software used in structural mechanics, it has the XFEM capabilities, Cast3M is developed by the Department of Modeling Systems and Structures of The French Alternative Energies and Atomic Energy Commission (CEA) [11], it uses the finite element method to solve different types of scientific problems. The calculation in Castem is done as follows:

1) Choice of the geometry and the mesh.
2) Definition of the mathematical and physical model: material properties, boundary conditions …
3) Solving of the problem: computation of stiffness and mass matrices, application of the loadings, solving.
4) Analysis and post-processing of the results.

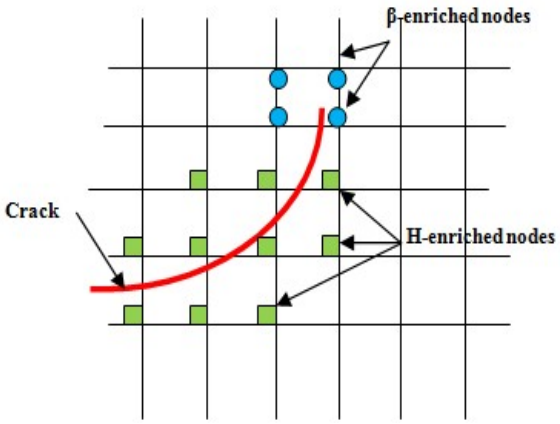

Fig. 1. The strategy of the enrichment in XFEM.

2.3. Governing equations

We consider an elastic solid subjected to surface forces or displacements, as well as volume forces (Fig. 2.), we look to determine the stresses and strains at each point. These physical quantities are expressed by tensors that are written in a matrix form.

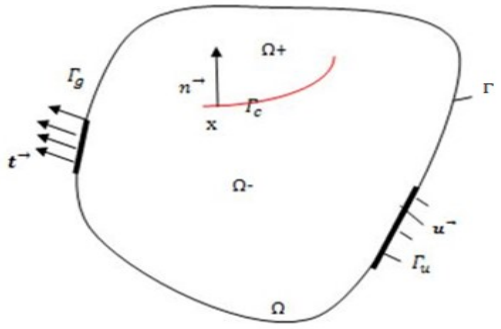

Fig. 2. Domain Ω with crack.

The parameter Γ is the outer boundary of the domain Ω with definition $\Gamma = \Gamma_u \cup \Gamma_g$. Traction t is imposed on the area Γ_g and displacement u is imposed on the area Γ_u (Fig. 2). In static, in the Cartesian coordinate system, the governing equations are given by the following relations:

$$\nabla\sigma + b = 0 \text{ or } (\sigma_{ij,j} + b_i) = 0 \quad \text{on the domain} \quad \Omega = \Omega^+ \cup \Omega^- \tag{4}$$

$$\sigma_{ij,j} n = t_i \quad \text{on} \quad \Gamma_g \tag{5}$$

$$U_i = u_i \quad \text{on} \quad \Gamma_u \tag{6}$$

$$\sigma_{ij,j} n = 0 \quad \text{on} \quad \Gamma_c \tag{7}$$

$$\varepsilon_{ij} = \frac{1}{2}(U_{i,j} + U_{j,i}) \tag{8}$$

where $\Omega \in \mathbb{R}^3$, $\vec{n}$ is a unit normal vector on the surface and b_i is the body force per unit volume. Γ_g, Γ_u and Γ_c are the traction, the displacement, and the crack boundaries respectively. Eq. (4) corresponds to the equilibrium equation where σ_{ij} is the Cauchy stress tensor at any point of the studied solid. Eqs. (5), (6) and (7) are obtained from the equilibrium on the surfaces (boundary conditions), t_i is the tensile force applied to the considered surface, U is the displacement field of displacements at any point on the solid surface. Eq. (8) is a geometric equation that defines the deformations in the hypothesis of small perturbations, ε_{ij} is the strain tensor at any point of the solid. In the numerical computation, we often look to minimize the elastic potential energy by defining the optimal stresses and strains. The software Castem [12] resolves the Eq. (9):

$$KU = f_{ext} \tag{9}$$

where U is the displacement vector, f_{ext} is the external force vector and K is the material stiffness matrix, they are given by Eqs. (10) and (11):

$$K = \int_{\Omega} B^T DB \; d\Omega \tag{10}$$

$$f_{ext} = \int_{\Omega} b \; d\Omega + \int_{\Gamma_g} t \; d\Gamma \tag{11}$$

The sub-matrices K_{ij} and f_i are obtained by substituting the approximation function defined in Eqs. (1), (10) and (11) [21]:

$$\begin{aligned} K_{ij} &= \begin{pmatrix} K_{ij}^{uu} & K_{ij}^{ua} & K_{ij}^{ub} \\ K_{ij}^{au} & K_{ij}^{aa} & K_{ij}^{ab} \\ K_{ij}^{bu} & K_{ij}^{ba} & K_{ij}^{bb} \end{pmatrix} \\ f_{iext}^{h} &= \left\{ f_i^u \; f_i^a \; f_i^{b_1} \; f_i^{b_2} \; f_i^{b_3} \; f_i^{b_4} \right\}^T \end{aligned} \tag{12}$$

The sub-matrices and vectors that appear in the foregoing equation (12) are given by:

$$K_{ij}^{kl} = \int_{\Omega} (B_i^k)^T D \, (B_j^l) d\Omega \quad \text{where } k,l = a,u,b \tag{13}$$

$$f_i^u = \int_{\Omega} N_i \; b_i \; d\Omega + \int_{\Gamma_g} N_i \; t_i \; d\Gamma \tag{14}$$

$$f_i^a = \int_{\Omega} N_i \; (H(x) - H(x_i)) \; b_i \; d\Omega + \int_{\Gamma_g} N_i \; (H(x) - H(x_i)) \; t_i \; d\Gamma \tag{15}$$

$$f_i^{b\alpha} = \int_{\Omega} N_i \; (\beta_\alpha(x) - \beta_\alpha(x_i)) \; b_i \; d\Omega + \int_{\Gamma_g} N_i \; (\beta_\alpha(x) - \beta_\alpha(x_i)) \; t_i \; d\Gamma \quad \text{where } \alpha = 1,2,3,4 \tag{16}$$

$$B_i^u = \begin{pmatrix} N_{i,x} & 0 & 0 \\ 0 & N_{i,y} & 0 \\ 0 & 0 & N_{i,z} \\ 0 & N_{i,z} & N_{i,y} \\ N_{i,z} & 0 & N_{i,x} \\ N_{i,y} & N_{i,x} & 0 \end{pmatrix} \tag{17}$$

$$B_i^a = \begin{pmatrix} N_i (H(x) - H(x_i))_{,x} & 0 & 0 \\ 0 & N_i (H(x) - H(x_i))_{,y} & 0 \\ 0 & 0 & N_i (H(x) - H(x_i))_{,z} \\ 0 & N_i (H(x) - H(x_i))_{,z} & N_i (H(x) - H(x_i))_{,y} \\ N_i (H(x) - H(x_i))_{,z} & 0 & N_i (H(x) - H(x_i))_{,x} \\ N_i (H(x) - H(x_i))_{,y} & N_i (H(x) - H(x_i))_{,x} & 0 \end{pmatrix} \tag{18}$$

$$B_i^u = \begin{pmatrix} N_{i,x} & 0 & 0 \\ 0 & N_{i,y} & 0 \\ 0 & 0 & N_{i,z} \\ 0 & N_{i,z} & N_{i,y} \\ N_{i,z} & 0 & N_{i,x} \\ N_{i,y} & N_{i,x} & 0 \end{pmatrix} \tag{19}$$

$$B_i^{b\alpha} = \left[B_i^{b1}, B_i^{b2}, B_i^{b3}, B_i^{b4} \right] \text{ with } \alpha = (1,2,3,4) \tag{20}$$

where N_i is the standard finite element (FE) function of node i, B_i is the matrix of shape function derivatives and calculated at the Gauss points of each element, $b_i(x)$ denotes the body force components, $t_i(x)$ is the tensile force applied to surface, Ω is the volume of the solid and Γ_g represents the traction boundary.

2.4. Crack meshing

In order to minimize the computation times, we used symmetry and modeled only a half-pipe with thickness transition and an external elliptical crack (Fig. 3a), we employed 2350 XFEM XC8R elements with 512 Gauss points in block crack, the size of the element in the crack is 0.15 (mm). For the rest of the mesh, we used 14950 standard elements CUB8 in the form of a hexahedron with 8 nodes (Fig. 3b). The pipes thickness variations are generally located at the outlet of reservoirs (valves) [14], therefore in boundary conditions, we fixed the displacement of the end of the thicker part of the pipe, in addition, we blocked the translation and the rotation in u_y and u_z axes by applying symmetry boundary conditions.

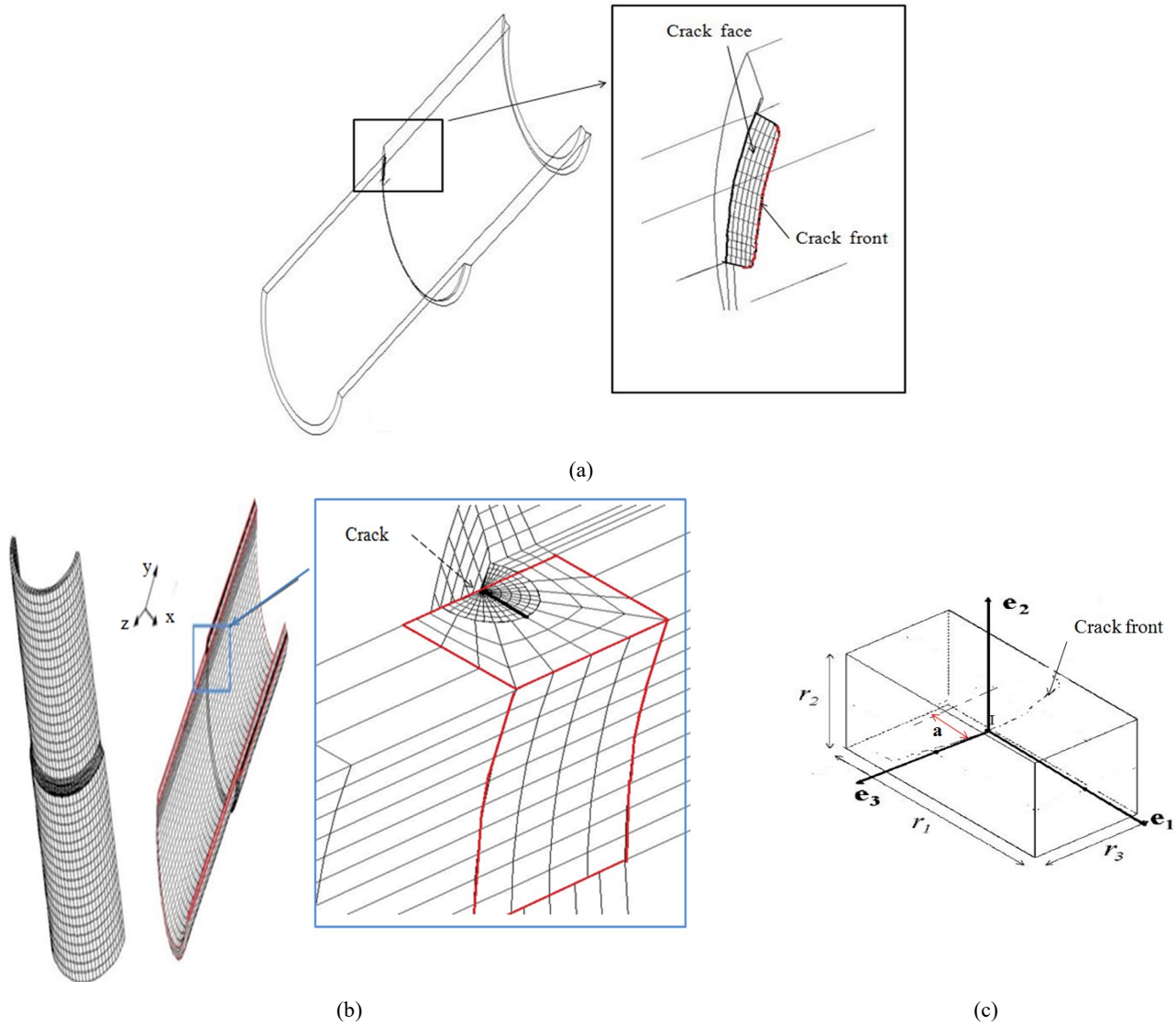

Fig. 3. (a) Meshing of elliptical crack, (b) cracked half –pipe with thickness transition, (c) the domain surrounding a segment of the crack front.

2.5. Enrichment zone

We defined the level sets by calculating them from the crack mesh, that is to say from a crack mesh we define a normal level set from the crack front (red bow Fig. 3a) and tangential level function from the crack face. The normal level set φ (PHI) gives the distance of a point x to the surface of the crack and the tangential level set ψ (PSI) gives the distance of a point x to the crack tip, these level functions define the crack as follows: for a point x of the solid (Fig. 4):

$$x \in \text{crack} \Rightarrow \begin{cases} \varphi(x)=0 \\ \psi(x)\leq 0 \end{cases} \quad \text{with } (|\nabla\psi| = |\nabla\varphi| = 1) \tag{21}$$

In FEM modeling, the works of refs. [3], [13] and [14] are based on a block of a semi-elliptical crack with complex geometry, whereas in XFEM modeling, for elastic-static fracture problems, the crack is easily modeled by enrichment functions using coarse and regular mesh (Figs 3a and 3b), the dimensions of the domain V of J integral, surrounding a segment of the crack front are taken as $r_1 = (35 + 0.06a)\ mm, r_2 = (2a - 0.2)\ mm$ and $r_3 = r_1/2$ where a is the depth of the crack in mm (Fig. 3c).

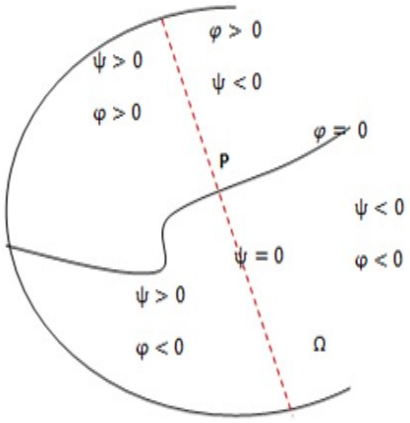

(a)

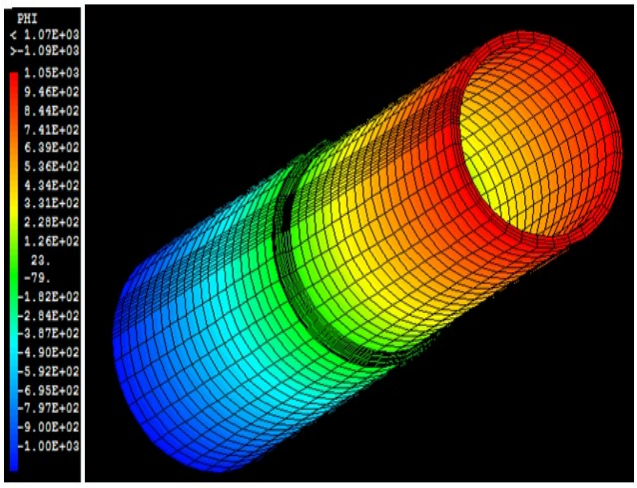

(b)

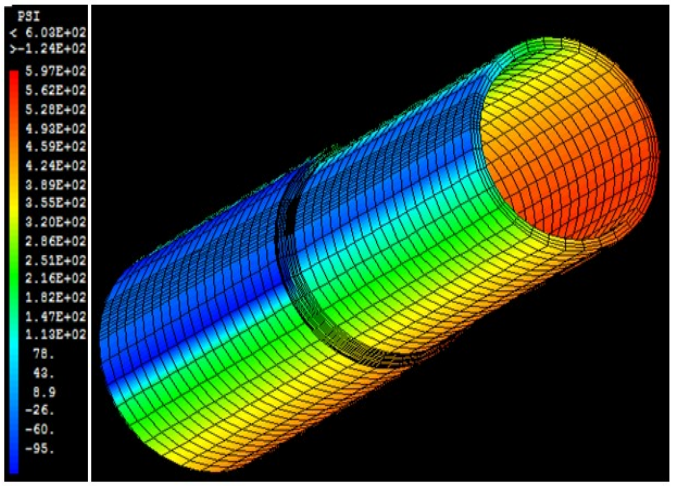

(c)

Fig. 4. (a) Representation of a crack with level sets, (b) normal level set, PHI, (c) tangential level set, PSI.

2.6. Calculation of SIF, (K) in XFEM

The parameter G corresponds to the energy dissipated for an infinitesimal crack advance, the G-theta is a method which calculates the J-integral in elastic-plastic behavior. The theoretical concept of J-integral was developed by Cherepanov [22] and Rice [23]. Rice [23] showed that the J-integral can be approached by the energy release rate G in the elastic range. For calculating the SIF, we consider a point I in crack front C, Γ_c presents a crack surface, it is composed with an outer surface Γ_c^+ and an inner surface Γ_c^-. In addition, V is a volume containing the crack front C (red arc in Fig. 5a) with is defined by $V = \Gamma_c^+ \cup \Gamma_c^- \cup \Gamma_0 \cup \Gamma_1 \cup \Gamma_2$. The level sets are used as a local basis at the crack front to describe the point I at all the volume V. Sukumar [24] has used the gradient of the level sets and defined this local basis (Fig. 6) by $e_1 = \nabla\psi$, $e_2 = \nabla\varphi$ and $e_3 = e_1 \Lambda e_2$.

In XFEM, J is expressed in a local basis (Fig. 6) formed of level set functions, J is given by Eq. (22) [16]:

$$J = \int_{\Gamma_c^+ \cup \Gamma_c^-} \theta_i \, P_{ij} \, n_j \, d\Gamma - \int_V \theta_i \, P_{ij} \, dV \tag{22}$$

where P_{ij} is the Eshelby tensor [25] given by Eq. (23):

$$P_{ij} = w\,\delta_{ij} - \sigma_{kj}\varepsilon_{ik} \quad (i,j,k) \in \{1,2,3\} \tag{23}$$

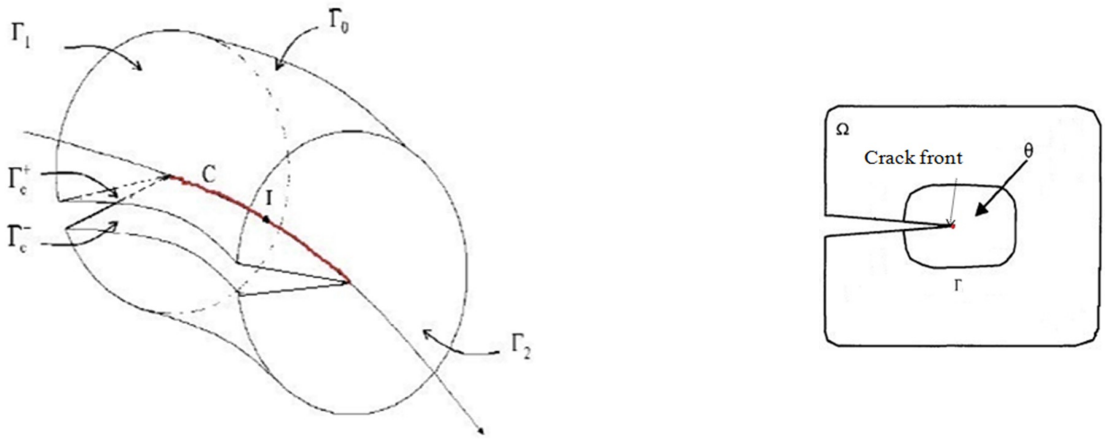

(a) (b)

Fig. 5. (a) The domain V in integral J computation, (b) example of θ field in two dimensions.

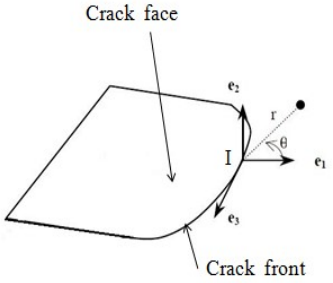

Fig. 6. Local basis on the crack front.

where w is the elastic energy density, σ and ε are respectively the stress and strain expressed in the basis (e_1,e_2,e_3) (Fig. 6). Furthermore, θ is a field of displacement parallel to the plane of the crack and normal to the front (Fig. 5b), it is defined by Eq. (24):

$$\theta = \mu e_1 \ , \ \mu(I) = 1 \text{ and } \mu(x) = 0 \quad \text{for} \quad x \in \Gamma_0 \cup \Gamma_1 \cup \Gamma_2 \tag{24}$$

For elastic behavior of materials, G is deduced from the J-integral by Eq. (25) [16]:

$$G = \frac{E}{2(1-\vartheta^2)} \times \frac{J}{\int_C \mu\, dC} \tag{25}$$

The SIF is deduced from G by Eq. (26) [16]:

$$G = \frac{K^2}{E'} \quad \text{with} \quad E' = \frac{E}{(1-\vartheta^2)} \quad \text{in plane strain} \tag{26}$$

3. Geometry and Loading

The study considered the elastic behavior of the material in P265GH steel, this material is especially used in pressure equipment, Table 1 presents the P265GH steel properties.

Table 1. The properties of P265GH steel.

Young's modulus, E (GPa)	Yield stress, σ (MPa)	Poisson's ratio, ϑ	Breaking stress, σ_u (MPa)	Nominal stress, f (MPa)
200	320	0.3	470	148

- The type of pipe is defined by the parameter t/R_i [13]:

$t/R_i > 0.1$: the pipe is thick.

$t/R_i < 0.1$: the pipe is thin.

$t/R_i = 0.1$: the pipe has an average thickness.

- The shape of the studied defect is semi-elliptic. It is characterized by the depth '*a*' and the total length '2*c*'. In order to study an extended configuration of the crack shapes, we used the parameter (*a*/*c*), this parameter defines elliptic crack elongation on the wall of the pipe. The parameter (*a*/*c*) gives several shapes of cracks: semi-circular crack for (*a*/*c*) = 1 to elongated elliptical crack for (*a*/*c*) = 1/8.
- In order to study an extended configuration of the types of defect, we used the parameter (*a*/*t*) to define the depth of the crack in the pipe wall, the parameter (*a*/*t*) gives several types of defect: shallow crack for (*a*/*t*) < 0.5 until deep crack for (*a*/*t*) = 0.8. We note that (*a*/*t*) is proportional to (*c*/*t*) where (*a*/*t*) = *x* (*a*/*t*) with *x* takes the values 1, 1/2, 1/4, and 1/8.

Therefore, the geometries of the considered cracked pipes are defined by dimensionless parameters:

- A fraction of thickness t on the inner radius of the pipe: t/R_i.
- Shape parameter defining elongation of the elliptical crack: (*a*/*c*).
- The depth of the defect standardized by the thickness of the tube: (*a*/*t*).

In the present paper, we model a pipe of average thickness ($t/R_i = 0.1$), the parameter (*a*/*c*) takes the values 1, 1/2, 1/4, and 1/8, (*a*/*t*) takes the values 0.1, 0.2, 0.4, 0.6, 0.8. This gives a set of 20 geometries. Elliptical cracks are considered to be located at the base of the transition in the thin part of the pipe (Figs. 3 and 7). The study deals with the straight pipe with thickness (*t*) and pipe with thickness transition (*t*, t_2) (Fig. 7). Pressurized pipe with thickness transition is a connection between pipe of thickness *t* assembled to another pipe of a thickness t_2 ($t_2 > t$) where the transition length respects the following relation defined by CODAP [26]:

$$l \le 0.2\sqrt{(2\times R_i + t_2)} \tag{27}$$

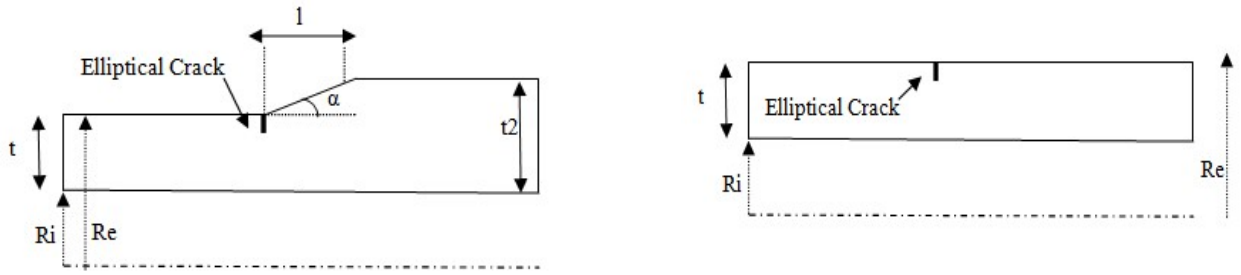

(a) (b)

Fig. 7. The geometry of pipes: (a) with thickness transition, (b) straight pipe.

The parameter (l) is the length of the transition zone, (α) is the slope of a pipe, and SIF (K) is the stress intensity factor. The purpose of this study is to investigate of the impact of (l) and (α) on the stress intensity in a pipe with thickness transition. So, we consider (l) and (α) as the variable parameters, and analyze their effect on SIF. Pipes are subjected to an internal pressure *P* (Fig. 8), for the purpose of comparison with the straight cylinder, the internal pressure is calculated in the thin part (thickness *t*) of the pipe with thickness transition, *P* is calculated according to the CODAP (C2.1.4.2) instructions [26]:

$$P = \frac{2\times f \times t \times z}{D_m} \tag{28}$$

where *z* is the welding coefficient, for an exceptional situation of service or resistance test, $z = 1, D_m = R_e + R_i$ is the inner dia meter of the pipe, R_i and R_e are respectively inner and outer radius of thin pipe where $R_e = t + R_i$. So, Eq. (28) becomes:

$$P\left(\frac{R_i}{t}\right) = \frac{2f}{2\left(\frac{R_i}{t}\right)+1} \quad \text{with} \quad \frac{R_i}{t} = 10 \tag{29}$$

The applied pressure, therefore, decreases with the decrease of the parameter t/R_i. The internal pressure is $P = 14$ *MPa*, this pressure respects the CODAP instructions [26], it does not cause the general plastic behavior in the pipe of average thickness ($t/R_i = 0.1$).

4. Results and Discussion

4.1 XFEM model verification

The Castem 2016 software [12] was used for modeling and calculation. It uses *G*-Theta method for calculating the integral *J* (*G* in elasticity) along the crack front (Eqs. 25 and 26).

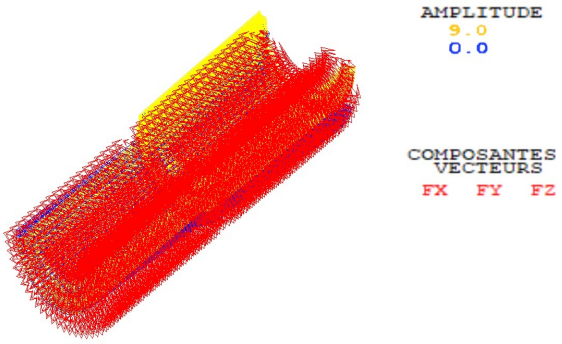

(a)

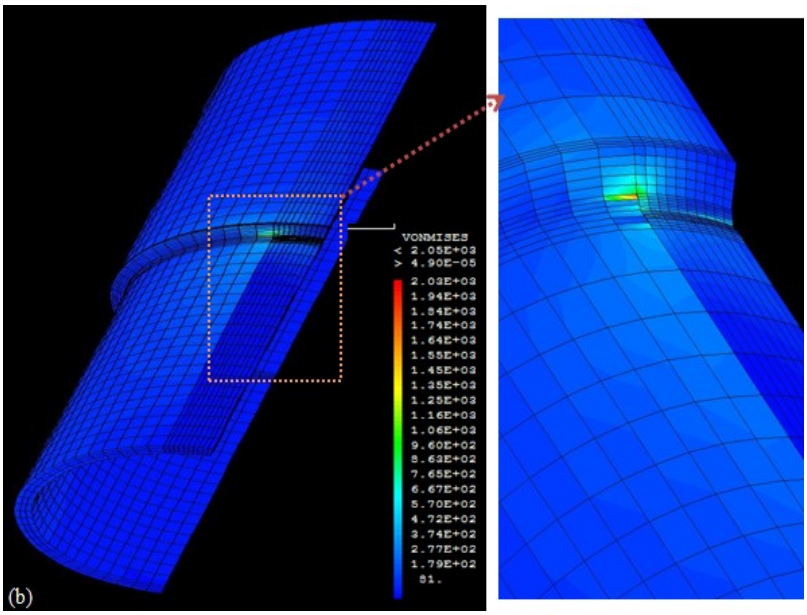

(b)

Fig. 8. Pipe with transition thickness: (a) subjected to internal pressure, (b) Von Mises stress.

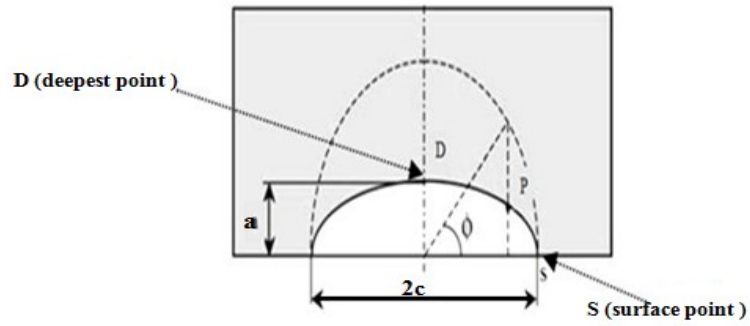

Fig. 9. Definition of angle ϕ.

The position of a point I on the crack front is defined by the angle ϕ (Fig. 9), ϕ takes the value of 90° at the deepest point (D) and 0° at the surface point (S). The semi-elliptical crack is characterized by two particular points: the deepest and the surface points (Fig. 9). In general, the evaluation of K at those two points is enough to judge the severity of the defect. At those points, the average value of K is given by Eqs. (30) and (31) (Fig. 10)[13]:

$$K_{average} = \frac{1}{5}(4K_{\text{point2}} + K_{\text{point3}}) \text{ in } D \text{ point} \tag{30}$$

$$K_{average} = \frac{1}{6}(K_{\text{point4}} + 4K_{\text{point5}} + K_{\text{point6}}) \text{ in } S \text{ point} \tag{31}$$

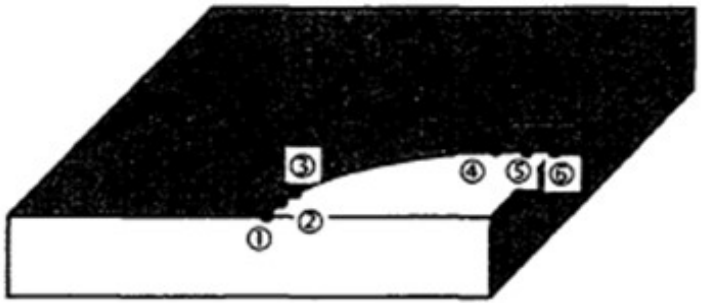

Fig. 10. Definition of average values on the element [13].

The French Alternative Energies and Atomic Energy (CEA) [11] has launched studies on uniform thickness pipes containing external circumferential cracks, based on the finite element method (FEM), CEA [11, 13] calculated the influence factor:

$$i_0 = \frac{K}{\dfrac{P R_i^2}{(R_e^2 - R_i^2)}\sqrt{\pi a}} \quad \text{for an external circumferential crack} \tag{32}$$

where P is the pressure calculated in Eq. (29) and K is the SIF calculated by the G-Theta method in XFEM. The influence function (i_0) is evaluated for an elliptical crack in a straight pipe, the verification of the model was made by the comparison of the values of i_0 calculated by XFEM in the present paper and the results from the literature [13]. The factor i_0 is calculated for all the fractions (a/c) and (a/t) at S and D points (Fig. 9). The relative error was calculated according to the Eq. (33):

$$e_1 = 100 \times \left| \frac{(i_{0_{CEA}} - i_{0_{XFEM}})}{i_{0_{CEA}}} \right| \tag{33}$$

Figs. 11 and 12 show the comparison results of i_0 respectively at D and S points calculated by XFEM and i_0 calculated by CEA [13] for all fractions (a/t) and (a/c). i_0 is also calculated along the crack front for all fractions (a/t) and (a/c), some comparison results are presented in Fig. 13. The relative error between the XFEM results and literature [13] is between 0.09% and 0.7%. There is a good concordance between the XFEM results and the value of [13], this gives confirmation to use numerical simulation based on XFEM to investigate the SIF at a thickness transition of pressurized pipe.

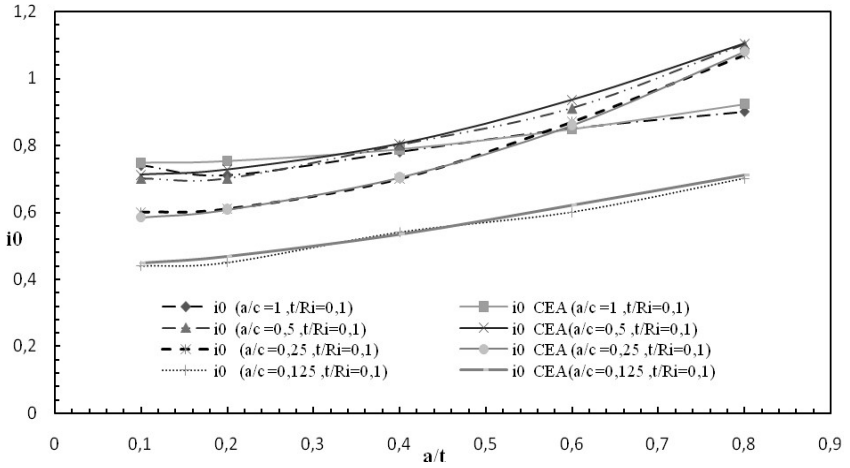

Fig. 11. Comparisons of i_0 calculated by XFEM in the present study with the literature [13], at S point, $t/R_i = 0.1$.

4.2. Effect of zone transition on SIF

In order to study the impact of (l) and (α) variations on the SIF, we consider (l) and (α) as variable parameters, and analyze their effect on SIF. Based on the triangular relation, the length of the thickness transition is related to the angle of the slope by the following relation:

$$l = \frac{(t_2 - t)}{\tan(\alpha)} \qquad \text{with} \qquad 0 < \alpha < \frac{\pi}{2} \tag{34}$$

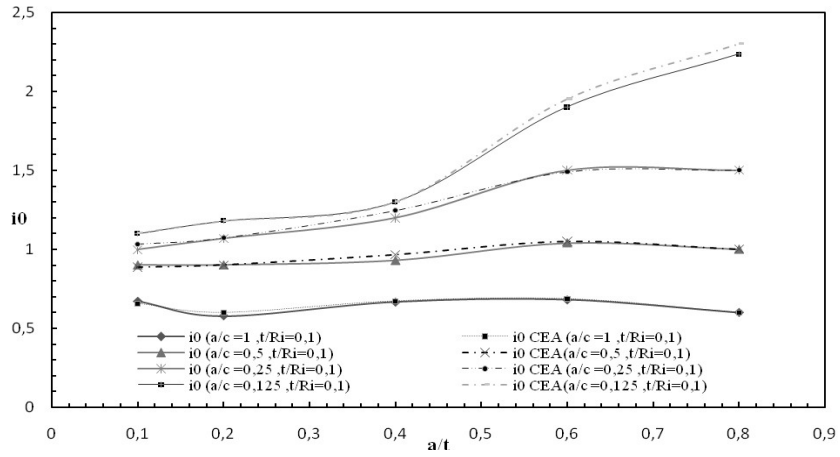

Fig. 12. Comparisons of i_0 calculated by XFEM in the present study with the literature [13], at *D* point, $t/R_i = 0.1$.

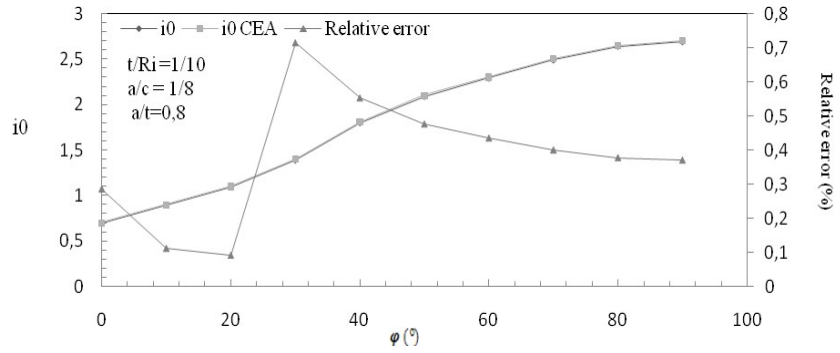

Fig. 13. Comparisons of i_0 calculated by XFEM in the present study with the literature [13], along the crack front.

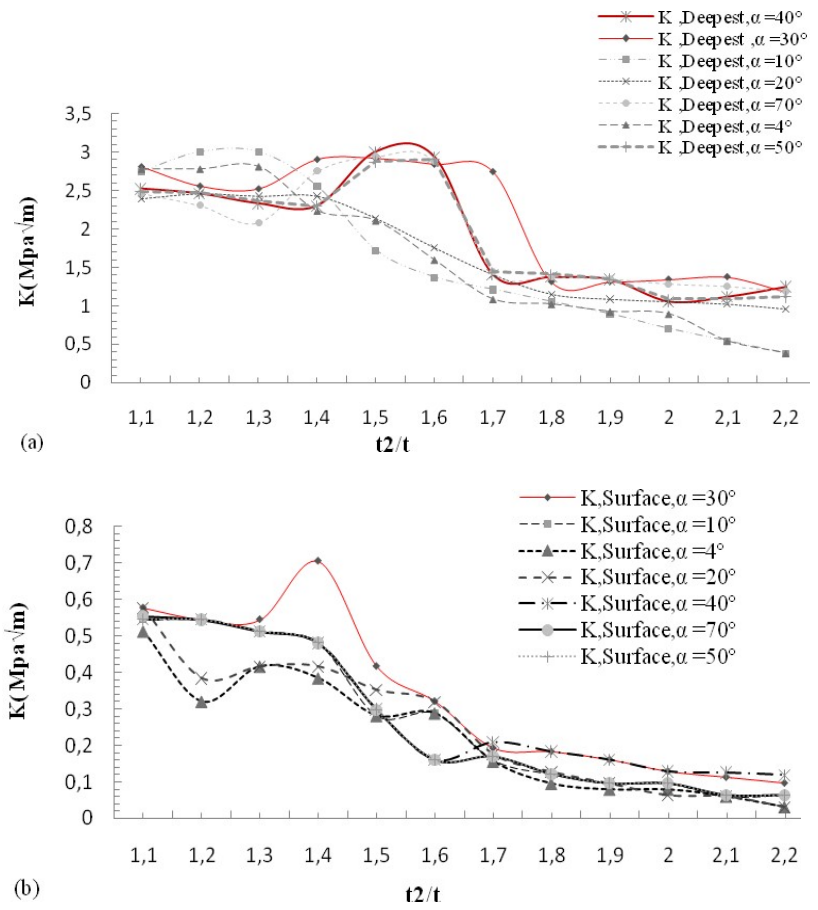

Fig. 14. Evolution of *K* value according to (t_2 / t) and (α): (a) for *D* point, (b) for *S* point.

The parameter (α) is varied within the range of 4° to 70° and the ratio (t_2/t) is varied from 1.1 to 2.1. Fig. 14 presents the variations of K according to the parameter (t_2/t), for certain slope (α) at D and S points. Fig. 14 shows that for both D and S points, we have:

- For $(\alpha) < 30°$, K increases when the angle (α) increases, K attains the maximum value for $(\alpha)=30°$, the general feature of the stress curve is unchanged for values of $\alpha > 30°$. In general, K decreases when (t_2/t) increases.
- For $(t_2/t) < 1.5$, K decreases when (t_2/t) increases, but K increases and attains its maximum for $(t_2/t)=1.5$ when $(\alpha)=30°$.
- For $(t_2/t) \geq 1.5$, K continues to decrease to become relatively stable and small.

To further show the effect of $(\alpha)=30°$ on the evolution of K, Fig. 15 presents the variations of K according to the parameter (l) for $\alpha = 30°$ at D and S points. It shows that K decreases when (l) increases.

- For 3mm $< (l) <$ 9mm, K is high and kepts a relatively constant value, for 9mm $< (l) <$ 30mm, K increases and attains its maximum for $(l) =$ 30mm ($(t_2/t) = 1.5$), but for $(l) >$ 30mm, K decreases again when (l) increases and takes a minimum value which is relatively constant for (l) between 45 and 70mm.

As a result, the angle $(\alpha) = 30°$ and $(t_2/t)=1.5$ are critical and grave cases of thickness transition in the pipe.

The decreasing of the angle of slope (α) and the increase of the parameter (t_2/t) is one effective method of reducing K.

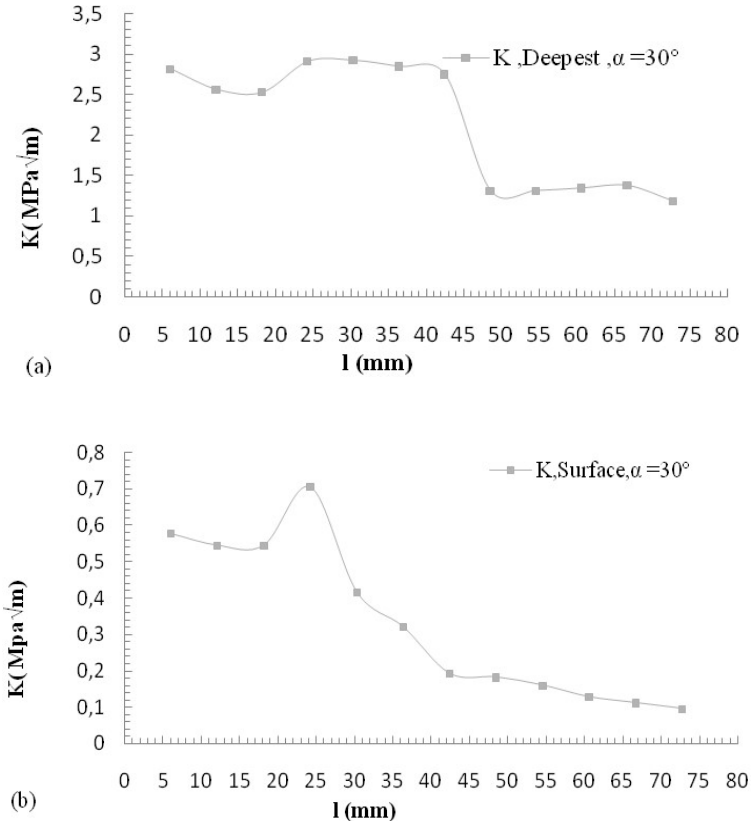

Fig. 15. Variations of the K value according to (l) (a) for D point, (α) = 30°, (b) for S point, (α)=30°.

4.3. Comparison between *K* of the pipe with uniform thickness and thickness transition using XFEM.

Considering the internal pressure, the present study compares the values of the SIF of an elliptical crack defect in straight pipe compared to one with thickness transition. The comparison was done by defining a parameter $\delta = K_T/K_C$, where K_C is the SIF calculated for straight pipe, and K_T is the SIF calculated for pipe with thickness transition. $\delta > 1$ means that the pipe with thickness transition presents more risk than a straight pipe. Fig. 16 shows the variations of δ according to (a/t) at D and S points for pipes where the parameter (t/R_i) is equal to 0.1.

- For the surface point (S):

-The value of δ does not depend on (a/c) parameter.

-The value of δ decreases when (a/t) increases, but it remains always greater than 1 for all parameters (a/c) and (a/t).

-The value of δ is maximum for shallow crack, where the K_T value is 2 times higher than K_C value, this means that a crack in the pipe with thickness transition presents double risk at a surface point in comparison with similar defects in a straight pipe.

- For the deepest point (D):

-The value of δ is sensitive to (a/c) fraction.

-The value of δ is greater than 1 for $a/t < 0.6$, K_T value is higher 4 to 6 times than K_C value for shallow crack.

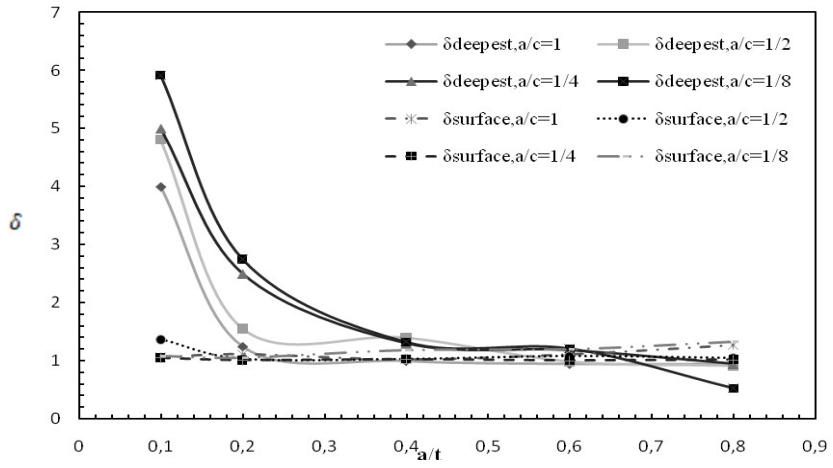

Fig. 16. δ values variation as function of a/c and a/t for internal pressure at the D and S points for $t / R_i = 0.1$.

We concluded that a similar defect in the thickness transition presents more risk compared to the straight pipe in the S point and D point for shallow crack ($a/t < 0.6$). The transition reacts as an amplifier of stress, it magnifies the stress close to the surface. When the depth of crack increases ($a/t > 0.6$), the concentration of the stress decreases at D point, because at D point, the impact of thickness transition noticeably reduces and the normal stress decreases until it becomes less than the constant stress on the straight pipe, therefore, the value of K at D point in thickness transition becomes smaller compared to the value of K in the straight pipe.

5. Conclusion

The present paper studied the effect of an external elliptical crack located at the thickness transition zone of a pipe. The study showed that the angle $\alpha = 30°$ and $t_2/t = 1.5$ are grave cases of the thickness transition pipe. The decreasing of the angle of slope and the increase of the length of the transition is one effective method of reducing the SIF. Considering the internal pressure, this work highlighted the study of a 3D crack problem in a thickness transition pipe using XFEM. In XFEM, level sets were defined. A crack is easily presented by enrichment functions. The comparison between the SIFs in straight pipes and pipes with thickness transition showed that the pipe containing thickness transition is more sensitive to the considered cracks. During the operation of pressure equipment, the pipes are exposed to plastic deformations, especially located near the crack tip, in perspective, we intend to evaluate the plastic behavior of the pressure pipe to study the 3D crack problem in thickness transition of pipe considering internal pressure.

Conflict of Interest

The author(s) declared no potential conflicts of interest with respect to the research, authorship and publication of this article.

Funding

The author(s) received no financial support for the research, authorship and publication of this article.

Nomenclature

a	Crack depth [mm]	l	Transition zone length [mm]
D point	The deepest point of the crack	S point	Surface point of the crack
G	Energy release rate, kJ/m^2	K, SIF	Stress intensity factor [MPa√m]
α	The angle of the slope of the pipe with thickness transition [◦]	t	The thickness of the pipe (thin side) [mm]
K_C	Stress intensity factor calculated for straight pipe [MPa√m]	t_2	The thickness of the pipe (thick side) [mm]
K_T	Stress intensity factor calculated for pipe with thickness transition [MPa√m]		

References

[1] Moustabchir, H., Elhakimi, A., Hariri, S., Azari,Z., Pressure study of gas transport pipes, in the presence of defects notch type, *18 ème Congrès Français de Mécanique*, Grenoble, 2007, 27-31.
[2] https://fr.wikipedia.org/wiki/Explosion_de_gaz_de_Ghislenghien.
[3] Hariri, S., El Hakimi, A., Azari, Z., Etude numérique et expérimentale de la nocivité des défauts dans des coques cylindriques et sphériques : aide à la détermination des facteurs de contraintes, *Revue de Mécanique Appliquée et Théorique*, 1(10), 2008, 1-10.
[4] Xiao, Z., Zhang, Y., Luo, J., Fatigue crack growth investigation on offshore pipelines with three-dimensional interacting cracks, *Geoscience Frontiers*, 9(6), 2018, 1689-1698.
[5] Idapalapati, S., Xiao, Z.M., Yi, D., Kumar, S.B., Fracture analysis of girth welded pipelines with 3D embedded cracks subjected to biaxial loading conditions, *Engineering Fracture Mechanics*, 96, 2012, 570-587.
[6] Broek, D., *Elementary engineering fracture mechanics*, Dordrecht: Kluwer, 1991.
[7] Gdoutos, E.E., *Fracture mechanics-an introduction*, Dordrecht: Kluwer, 1991.
[8] Le Grognec, P., Hariri, S., Afzali, M., Jaffal, H., Nocivité des défauts et propagation de fissures dans les équipements sous pression, *18 ème Congrès Français de Mécanique*, 2007.
[9] Sabokrouh, M., Farahani, M., Experimental Study of the Residual Stresses in Girth Weld of Natural Gas Transmission Pipeline, *Journal of Applied and Computational Mechanics*, 5(2), 2019, 199-206.
[10] Vakili Tahami, F., Biglari, H., Raminnea, M., Optimum Design of FGX-CNT-Reinforced Reddy Pipes Conveying Fluid Subjected to Moving Load, *Journal of Applied and Computational Mechanics*, 2(4), 2016, 243-253.
[11] The French Alternative Energies and Atomic Energy Commission (CEA). 'Commissariat a` L'Energie Atomique (France).
[12] http://www-cast3m.cea.fr/.
[13] Chapuliot, S., Lacire, M.H., Stress intensity factors for external circumferential cracks in tubes over a wide range of radius over thickness ratios. American Society of Mechanical Engineers, Pressure Vessels and Piping Division (Publication), 365, 1999, 95-106.
[14] Saffih, A., Hariri, S., Numerical study of elliptical cracks in cylinders with a thickness transition, *International Journal of Pressure Vessels and Piping*, 83, 2006, 35-41.
[15] Le Delliou, Calcul simplifié du paramètre J pour un défaut axisymétrique débouchant en surface externe d'une transition d'épaisseur.
[16] Moës, N., Gravouil, A., Belytschko, T., Non-planar 3D crack growth by the extended finite element and level sets; Part I: Mechanical model, *International Journal for Numerical Methods in Engineering*, 53, 2002, 2549-2568.
[17] Medinas, M.T.L.F., *An Extended Finite Element Method (XFEM) approach to hydraulic fractures: Modelling of oriented perforations*, Master Thesis, Tecnico Lisboa, 2015.
[18] Belytschko, T., Black, T., Elastic crack growth in finite elements with minimal remeshing, *International Journal for Numerical Methods in Engineering*, 45, 1999, 601–620.
[19] Stolarska, M., Chopp, D., Moes, N., Belytschko, T., Modelling crack growth by level sets in the extended finite element method, *International Journal for Numerical Methods in Engineering*, 51, 2001, 943–960.
[20] Kamal Sharma, I., Singh, V., Mishra, B.K., Bhasin, V., Numerical Modeling of Part-Through Cracks in Pipe and Pipe Bend using XFEM, *Procedia Materials Science*, 6, 2014, 72-79.
[21] Kumar, S., Singh, I.V., Mishra, B.K., A coupled finite element and element-free Galerkin approach for the simulation of stable crack growth in ductile materials, *Theoretical and Applied Fracture Mechanics*, 70, 2014, 49-58.
[22] Cherepanov, G.P., The propagation of cracks in a continuous medium, *Journal of Applied Mathematics and Mechanics*, 31(3), 1967, 503-512.
[23] Rice, J.R., A Path Independent Integral and the Approximate Analysis of Strain Concentration by Notches and Cracks, *Journal of Applied Mechanics*, 35, 1968, 379-386.
[24] Sukumar, N., Chopp, D.L., Moran, B., Extended finite element method and fast marching method for three-dimensional fatigue crack propagation, *Engineering Fracture Mechanics*, 70, 2003, 29-48.
[25] Eshelby, J.D., The Continuum Theory of Lattice Defects, *Solid State Physics*, 3, 1956, 79-144.
[26] French construction code. Construction des Appareils à Pression non soumis à l'action de la flamme, 'the Code for Construction of unfired Pressure Vessels, Division 1, part C – design and calculation, section C2 – rules for calculating cylindrical, spherical and conical shell subjected to internal pressure, 2005, 539-622.